The Astrophysical Journal, 884:35 (12pp), 2019 October 10 https://doi.org/10.3847/1538-4357/ab4128

Exploring the Cycle Period and Parity of Stellar Magnetic Activity with Dynamo Modeling

Gopal Hazra[1,2], Jie Jiang[1], Bidya Binay Karak[3], and Leonid Kitchatinov[4,5]
[1] School of Space and Environment, Beihang University, Beijing, People's Republic of China; jiejiang@buaa.edu.cn
[2] School of Physics, Trinity College Dublin, the University of Dublin, Dublin-2, Ireland
[3] Department of Physics, Indian Institute of Technology (Banaras Hindu University), Varanasi, India
[4] Institute for Solar-Terrestrial Physics, Lermontov Str. 126A, 664033, Irkutsk, Russia
[5] Pulkovo Astronomical Observatory, St. Petersburg, 196140, Russia
Received 2019 April 18; revised 2019 August 7; accepted 2019 September 2; published 2019 October 11

Abstract

Observations of chromospheric and coronal emissions from various solar-type stars show that the stellar magnetic activity varies with the rotation rates of the stars. The faster the star rotates, the stronger its magnetic activity becomes, but the activity cycle period does not show a straightforward variation with the rotation rate. For slowly rotating stars, the cycle period decreases with the increase in rotation rate, while for the fast rotators, the dependency of cycle period on rotation is presently quite complicated. We aim to provide an explanation of these observational trends of stellar magnetic activity using a dynamo model. We construct a theoretical dynamo model for stars of mass 1 $M_\odot$ based on the kinematic flux transport dynamo model including radial pumping near the surface of the stars. The inclusion of this near-surface downward radial pumping is found to be necessary to match the observed surface magnetic field in the Sun. The main ingredients of our dynamo model, meridional circulation and differential rotation for stars, are obtained from a mean-field hydrodynamic model. Our model shows a decrease in cycle period with increasing rotation rate in the slowly rotating regime and a slight increase in cycle period with rotation rate for the rapid rotators. The strength of the magnetic field is found to increase as the rotation rate of the star increases. We also find that the parity of the stellar magnetic field changes with rotation. According to our model, the parity flips to quadrupolar from dipolar if the rotation period of the star is less than 17 days.

Key words: stars: activity – stars: magnetic field – stars: rotation – stars: solar-type

1. Introduction

Many solar-type stars with an outer convection zone (CZ) show cyclic magnetic behavior like the 11 yr cycle of the Sun. Unlike the Sun, for which long-term photospheric measurements of the magnetic field and its proxies are available, however, stellar observations are limited. It has been realized that magnetic (nonthermal) heating in the chromosphere causes emission from the core of Ca II H and K lines. This H and K emission is shown to have a strong correlation with the magnetic flux, as realized in the Sun (Skumanich et al. 1975; Schrijver et al. 1992). Therefore, the H and K emission flux is taken as a measure of the stellar magnetic activity. While the magnetic activity, in general, is expected to correlate with the rotation rates of stars, Noyes et al. (1984a) showed that the activity correlates better with the Rossby number (Ro), which is a ratio of the rotation period to the convective turnover time. As seen in Figure 8 of Noyes et al. (1984a), the activity first increases rapidly, and then the activity increases very slowly or even seems to be independent of Ro. Combining data for coronal X-ray emission, which is also taken as a proxy for the stellar magnetic field, of more than 800 solar-type stars, Wright et al. (2011) and Wright & Drake (2016) find a rotation–activity relation similar to that seen in the Ca II H and K data. Like the magnetic activity, the magnetic cycle period also depends on the rotation rate of the star. By analyzing Ca II H and K data of a homogeneous sample of older, slowly rotating stars, Noyes et al. (1984b) found that the cycle period ($P_{\rm cyc}$) increases as the rotation period ($P_{\rm rot}$) of the star increases. Later, many other studies (Saar & Brandenburg 1999; Saar 2002; Böhm-Vitense 2007) also found similar results in which the cycle period increases with increasing rotation period across the different activity branches of stars (e.g., see Figure 1 of Böhm-Vitense 2007; the cycle period increases with increasing rotation period along the inactive and active branches). This increasing trend of cycle period with rotation period is the so-called $P_{\rm cyc}$–$P_{\rm rot}$ relation. Recently, Boro Saikia et al. (2018) analyzed data from 4454 cool stars from various surveys and pointed out that not all stars in their sample follow this relation. Using their robust period-detection algorithm, they classified the sample of stars into three different segments: stars with well-defined cycles, stars with multiple cycles, and stars with an unconfirmed cycle. The stars with well-identified cycle periods show an increasing trend in cycle period with increasing rotation period, and most of them are slow rotators belonging to the inactive branch. However, uncertainties lie in the stars on the fast-rotating branch, which show multiple chaotic cycles. This result is also supported by Olspert et al. (2018), who have done an individual probabilistic analysis of the Ca II H and K data. Another important property of stellar magnetic activity is the global parity of the magnetic field, which determines the angular momentum loss that is due to the magnetized stellar wind (Réville et al. 2015). Although the solar magnetic field is dipolar (Hale et al. 1919; Stenflo 1988; DeRosa et al. 2012), we do not have information on the magnetic parity of other stars.

Efforts to understand the observed empirical activity–rotation relation and $P_{\rm cyc}$–$P_{\rm rot}$ relation started early using mean-field dynamo models (Durney & Robinson 1982; Robinson & Durney 1982; Noyes et al. 1984a, 1984b). In recent years, Babcock–Leighton (BL)-type kinematic dynamos, also known as flux transport dynamo models, have become popular models for the solar cycle because of their success in reproducing many aspects

of the solar magnetic cycle (Babcock 1961; Leighton 1969; Choudhuri et al. 1995; Durney 1995; Dikpati & Charbonneau 1999); also see reviews by Charbonneau (2010), Choudhuri (2011), and Karak et al. (2014a). These models are kinematic in the sense that velocity fields are provided from observations and the nonlinear feedback due to Lorentz force is not considered in general. The mean flows, for example differential rotation and meridional circulation, play the most important role in amplifying and transporting the magnetic fields. Two major components of this model, namely, the generation of the toroidal field through differential rotation (the Ω effect) and the generation of the poloidal field from the decay and dispersal of tilted bipolar active regions (the BL process), are observationally supported (Dasi-Espuig et al. 2010; Kitchatinov & Olemskoy 2011b; Muñoz-Jaramillo et al. 2013; Priyal et al. 2014; Cameron & Schüssler 2015). In the BL process, the tilt of the bipolar active region is crucial in determining the strength of the poloidal field (Jiang et al. 2014, 2015). This tilt is believed to be caused by the Coriolis force acting on the rising flux tube in the CZ (D'Silva & Choudhuri 1993). Thus, it is expected to increase with the rotation rate of the star. Thereby, the magnetic field in the BL dynamo model also should increase with the rotation rate.

The main difficulty in extrapolating the flux transport model for the stellar case is less availability of observed mean flows. For the Sun, we have good data of differential rotation and some data of meridional circulation from helioseismology, and that is why observational data-driven models are very close to explaining various observational features of the Sun. Although we have some evidence of differential rotation at the surface of stars (Barnes et al. 2005; Berdyugina 2005; Strassmeier 2009), detailed information throughout their CZs is not available. For stellar meridional circulation, we have almost no available data. Detailed information on mean flows inside the stellar CZ is necessary to construct a realistic dynamo model of stars. Therefore, we have to rely on a theoretical analysis to get the differential rotation and meridional circulation in stars. One way to get the mean flows for solar-type stars is to solve jointly the mean-field equation of motion with the heat transport equation (Kitchatinov & Ruediger 1995; Küker & Stix 2001; Rempel 2005; Hotta & Yokoyama 2011; Kitchatinov & Olemskoy 2011a). Another way is to solve the full Navier–Stokes equation, including the heat transport equation, directly, which is done in global hydrodynamic and magnetohydrodynamic simulations (e.g., Miesch 2005; Brown et al. 2008; Racine et al. 2011; Käpylä et al. 2016; Karak et al. 2018). The mean-field model of Kitchatinov & Olemskoy (2011a) calculates the differential rotation of main-sequence dwarfs having different masses and different rotation periods. The meridional circulation automatically comes out in this model, as a consequence of angular momentum balance. When this model is implemented for solar-type stars with a solar rotation period, it gives rise to a differential rotation that is very close to the helioseismology result. This model also gives a single-cell meridional circulation encompassing the whole CZ, with a poleward flow at the surface and an equatorward flow near the bottom of the CZ. We have used this model to obtain the mean flows of solar-type stars to incorporate them into all of our dynamo calculations.

Some of the previous attempts (Jouve et al. 2010; Dubé & Charbonneau 2013), who extrapolated the flux transport dynamo models for the stellar case, have used the mean flows computed from the 3D global hydrodynamic simulations of the stars (Brown et al. 2008; Racine et al. 2011; Guerrero et al. 2013). Karak et al. (2014b) used the mean flows from the mean-field hydrodynamic model of Kitchatinov & Olemskoy (2011a). The activity–rotation relation has been demonstrated in these previous flux transport dynamo models for solar-type stars (Jouve et al. 2010; Karak et al. 2014b; Kitchatinov & Olemskoy 2015). However, these models were not able to reproduce the decreasing trend of cycle period with increase in rotation rate as seen in the observations of slowly rotating stars. In the flux transport dynamo model, the cycle period is inversely proportional to the speed of the meridional circulation (Dikpati & Charbonneau 1999; Karak 2010). The meridional circulation, on the other hand, decreases with the increase in rotation rate (as seen in the previous studies that with the increase in rotation rate, the energy in the azimuthal motion increases rapidly and decreases the energy in the meridional motion; Miesch 2005; Brown et al. 2008; Karak et al. 2015). Thus, these models give longer cycle periods for highly rotating stars in contrast to the observations. In summary, the flux transport dynamo, although it reproduced the observed stellar activity–rotation qualitatively, failed to reproduce the correct $P_{\rm cyc}$–$P_{\rm rot}$ relation, at least for the slowly rotating stars (see Brun 2014; Choudhuri 2017, for detailed discussion). The scenario becomes different if turbulent pumping is included in the model (Do Cao & Brun 2011). Recent global convective simulations also were not able to get the correct trend for cycle period and sometimes get the opposite trend, specifically for the slow rotators (Strugarek et al. 2017; Warnecke 2018).

The pumping is unavoidable in a stratified stellar CZ due to the topological asymmetric convective flow (Tobias et al. 2001; Käpylä et al. 2006; Miesch & Hindman 2011). Previous studies have shown that pumping is very important in transporting the poloidal field from the surface to the deeper CZ (Guerrero & de Gouveia Dal Pino 2008; Karak & Nandy 2012). Cameron et al. (2012) and Jiang et al. (2013) showed that a downward radial pumping in the near-surface shear layer is essential in the flux transport dynamo model to match the results with the properties of the observed surface magnetic field. Karak & Cameron (2016) have shown that the pumping increases the dynamo efficiency by suppressing the diffusion of the magnetic field across the surface. Thus pumping helps to produce a 11 yr magnetic cycle even with very high diffusivity in the CZ and also helps the dynamo to recover from Maunder-like extended grand minima of weaker activity (Karak & Miesch 2017, 2018).

The aim of our paper is to explore the $P_{\rm cyc}$–$P_{\rm rot}$ relation using a flux transport dynamo model with added downward radial turbulent pumping. We shall show that the behavior of the stellar magnetic cycles with the radial pumping will be different than that obtained in previous flux transport dynamo models. With this model, we shall show that $P_{\rm cyc}$ decreases with decreasing $P_{\rm rot}$ of the stars, and after a certain rotation period, it starts to increase. We will compare these results with the available stellar observations. We shall also predict the parity of the magnetic field in rapidly rotating stars. We shall show that when the rotation rate is faster than a certain value, the parity becomes quadrupolar instead of dipolar, which is the dominant parity of the solar magnetic field. In the next section, we discuss our model and model parameters in detail. In Section 3 we present and discuss our results. Finally, our conclusions are summarized in Section 4.

2. Model

We adopt the flux transport dynamo model to construct a dynamo model for solar-type stars. In this model, the total magnetic field is assumed to be axisymmetric and consists of toroidal and poloidal components, which can be written as

$$\boldsymbol{B}_{\rm tot}(r,\,\theta,\,t) = B(r,\,\theta,\,t)\hat{\boldsymbol{e}_\phi} + \nabla \times A(r,\,\theta,\,t)\hat{\boldsymbol{e}_\phi}. \quad (1)$$

The following equations govern the behavior of the poloidal field ($\boldsymbol{B}_p = \nabla \times A(r,\,\theta,\,t)\hat{\boldsymbol{e}}_\phi$) and toroidal field ($B$) with time:

$$\frac{\partial A}{\partial t} + \frac{1}{s}(\boldsymbol{v}.\nabla)(sA) = \eta_t\left(\nabla^2 - \frac{1}{s^2}\right)A + S_{\rm BL}(r,\,\theta;\,B), \quad (2)$$

$$\frac{\partial B}{\partial t} + \frac{1}{r}\left[\frac{\partial}{\partial r}(rv_r B) + \frac{\partial}{\partial \theta}(v_\theta B)\right] = \eta_t\left(\nabla^2 - \frac{1}{s^2}\right)B + s(\boldsymbol{B}_p.\nabla)\Omega + \frac{1}{r}\frac{d\eta_t}{dr}\frac{\partial B}{\partial r}, \quad (3)$$

where $s = r\sin\theta$, $S_{\rm BL}$ is the source function, which captures the effect of the BL mechanism on the surface of the stars, and η_t is the turbulent diffusivity, and other terms are in usual notation. We want to solve these dynamo equations for different solar-type stars with velocity profiles obtained from the mean-field hydrodynamic models of flows. All of the model parameters that we have used in our model to understand stellar magnetic activity are described in detail below. We want to point out that our model is somewhat different than the previous model used by Karak et al. (2014b). First of all, a radial downward turbulent pumping is used in our model near the surface of the stars, and the turbulent diffusivity is higher than the profile that Karak et al. (2014b) used. We kept the boundary condition for the magnetic field completely radial at the surface. The radial pumping near the surface and vertical field boundary conditions are required for the results of the flux transport dynamo models to match with the observation more closely (Cameron et al. 2012; Jiang et al. 2013). The downward pumping profile mainly contributes in the advection of the poloidal field downward and less diffusion of fields through the surface.

2.1. Meridional Circulation and Differential Rotation of Stars

We have used the same meridional circulation and differential rotation as used by Karak et al. (2014b) from the model of Kitchatinov & Olemskoy (2011a). Three joint equations for angular velocity, meridional flow, and entropy are solved in the CZ of a solar-type star to get the mean flows in this model. The computations give solar-type differential rotation with the equator rotating faster than the poles for all stars that we consider in the present calculations. The differential profiles for some of the stars with rotation periods of 30 days, solar, 15 days, and 1 day are given in Figure 1. Meridional circulations for those stars are also shown in Figure 2. The meridional circulations consist of a single cell with a poleward flow at the surface and an equatorward flow at the bottom of the CZ. For all stars, meridional circulation has a penetration depth of $0.7R_\star$. Also note that as the rotation rate of a star increases, the meridional circulation becomes more confined near the boundaries of the CZ; see Figure 4 of Karak et al. (2014b).

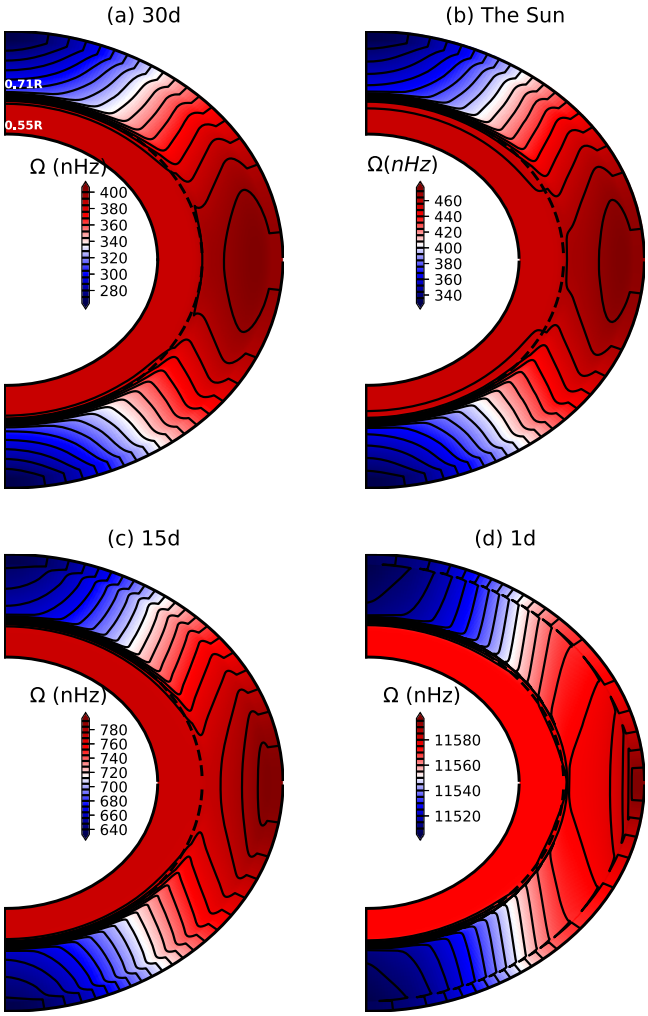

Figure 1. Differential rotation computed from the Kitchatinov & Olemskoy (2011a) model for stars with rotation period of (a) 30 days, (b) solar, (c) 15 days, and (d) 1 day.

2.2. Turbulent Diffusivity and Turbulent Pumping

In most of the flux transport dynamo models, an order of magnitude less turbulent diffusivity than what mixing length theory estimates has been used (see Figure 4 of Karak & Cameron 2016). Here we use a significantly high diffusivity that is close to the mixing length estimation and the observationally motivated value of Cameron & Schüssler (2016). The magnetic diffusivity that we have used for all our simulations is

$$\eta_t = \eta_c + \frac{\eta_{\rm mid}}{2}\left[1 + {\rm erf}\left(2\frac{r - 0.7R_\star}{0.03R_\star}\right)\right] + \frac{\eta_{\rm top}}{2}\left[1 + {\rm erf}\left(\frac{r - 0.90R_\star}{0.05R_\star}\right)\right], \quad (4)$$

where $\eta_c = 7.5 \times 10^9\,{\rm cm^2\,s^{-1}}$, $\eta_{\rm mid} = 7.5 \times 10^{11}\,{\rm cm^2\,s^{-1}}$, and $\eta_{\rm top} = 3 \times 10^{12}\,{\rm cm^2\,s^{-1}}$.

Following Cameron et al. (2012), Karak & Cameron (2016), and Karak & Miesch (2018), we use the following radial

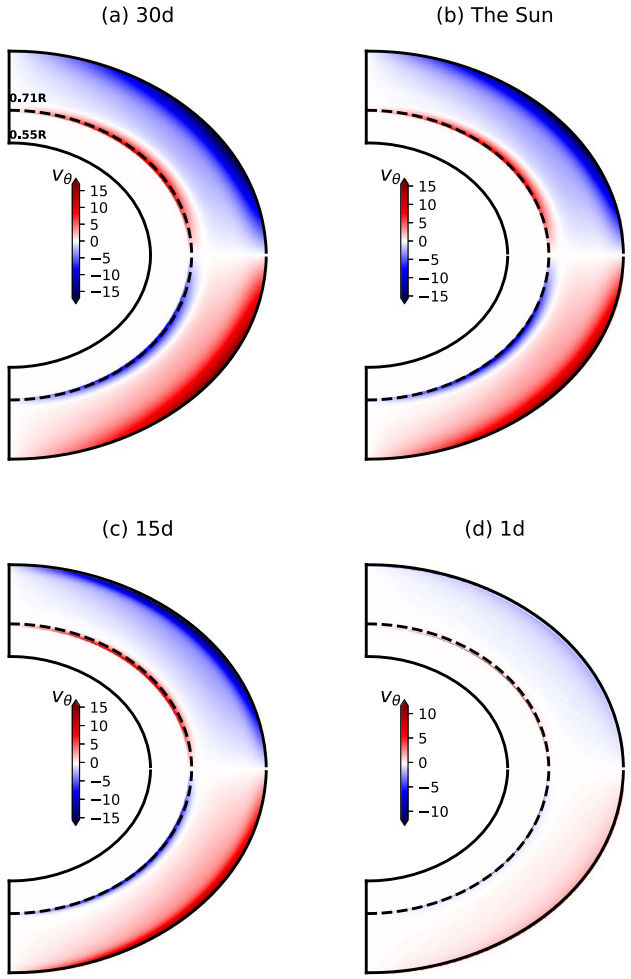

Figure 2. Same as Figure 1, but for the latitudinal component of meridional circulation. All units are in m s^{-1}.

pumping profile near the surface:

$$\gamma_r = -\frac{\gamma_0}{2}\left[1 + \mathrm{erf}\left(\frac{r - 0.9R_\star}{0.02R_\star}\right)\right], \quad (5)$$

where γ_0 sets up the amplitude of the magnetic pumping, which is fixed to 24 m s^{-1} in all of the simulations unless otherwise mentioned. Note that the choice of γ_0 value is somewhat arbitrary at present (Cameron et al. 2012; Karak & Cameron 2016), and we choose $\gamma_0 = 24$ m s^{-1} because, for the solar case, it gives results that are very close to observations. The profiles of η_t and γ_r are shown in Figure 3. To be more specific, the idea of incorporating turbulent pumping is to suppress the diffusive decay of the magnetic field through the surface of the stars, and to complete this task we need the near-surface magnetic Reynolds number $R_m = \frac{|v_p|L}{\eta} > 1$, which implies velocity $v_p > \frac{\eta}{L}$.

Assuming $\eta = \frac{\eta_{\rm top} + \eta_{\rm mid}}{2}$ and $L = 2\pi R_\star$, the amplitude of the pumping (v_p) should be approximately at least more than 5 m s^{-1} for $R_m > 1$. Cameron et al. (2012) performed a series of simulations with different pumping amplitudes and estimated that a strong downward pumping speed of 25 m s^{-1} is needed in order to match the results of the flux transport dynamo simulation with the observed solar polar fields. Different radial

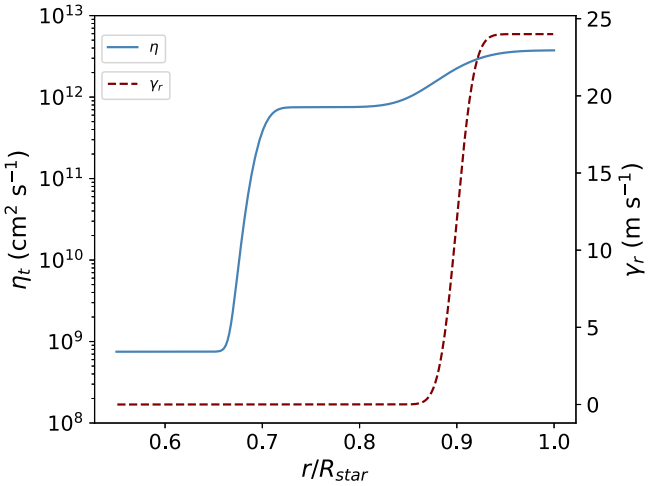

Figure 3. The blue solid line shows the turbulent diffusivity used in our simulations, and the dark-red dashed line shows the downward radial pumping near the surface (right y axis shows the amplitude of the pumping).

pumping profiles have been used by different groups to mimic the downward transport of the fields (Guerrero & de Gouveia Dal Pino 2008; Karak & Nandy 2012; Kitchatinov & Olemskoy 2012). Many of the profiles were confined inside the whole CZ, but we have used a downward pumping profile near the surface layers (Cameron et al. 2012; Karak & Cameron 2016) because radial pumping is most significant there due to very high density stratification, which is consistent with the numerical simulations (Miesch & Hindman 2011).

2.3. Babcock–Leighton α

This is an essential process to generate the poloidal field from the toroidal field in our model, and this process is mainly confined near the surface of the Sun. The source term ($S_{\rm BL}$) in Equation (2) incorporates this BL process and can be written as

$$S_{\rm BL}(r, \theta, t) = \frac{\alpha B(r_t, \theta, t)}{1 + [B(r_t, \theta, t)/B_0]^2}, \quad (6)$$

where $B(r_t, \theta, t)$ is the value of the toroidal field averaged over the tachocline from $r = 0.685R_\star$ to $r = 0.715R_\star$. Here, B_0 is the quenching field strength, and this is the only nonlinearity considered in our model. All of the magnetic field strengths are given in the units of B_0. We have used the following α profile, in which we make sure that it should be confined in the upper layers of the CZ:

$$\alpha = \frac{\alpha(\Omega) f(\theta)}{2}\left[1 + \mathrm{erf}\left(\frac{r - 0.95R_\star}{0.01R_\star}\right)\right]. \quad (7)$$

Depending on the rotation rate of a star, the amplitude of the α profile and its latitudinal extent vary. The $\alpha(\Omega)$ determines the strength of the BL mechanism, and $f(\theta)$ considers the latitudinal extent of starspot emergence. For rapidly rotating stars, we expect the buoyant rise of the toroidal flux tube along the rotation axis and that polar spots would appear in the high-latitude regions (Schuessler & Solanki 1992; Jeffers et al. 2002; Waite et al. 2015; Işık et al. 2018). Hence, the BL process would be stronger in the high-latitude regions of those stars. We have considered two different cases based on two different

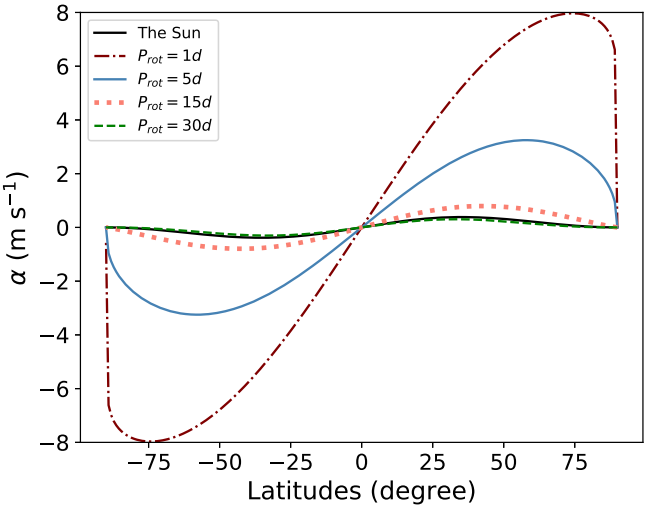

Figure 4. Latitudinal variation of the α profile for stars with different rotation periods for Case II (Equation (9)). The solid black line shows the standard solar case. As a star rotates faster than the Sun, the corresponding α becomes larger and more concentrated toward high latitudes. The dash-dotted brown line, blue solid line, dotted orange line, and dashed green line show the α profile for stars rotating with rotation periods of 1, 5, 15, and 30 days, respectively.

dependencies of rotation on (1) the strength of the BL process $\alpha(\Omega)$ and (2) its latitudinal extent $f(\theta)$.

First, we have considered the strength of the α effect as a simple function of rotation and kept the latitudinal extent the same as for the standard solar case.

Case I:

$$\alpha(\Omega) = \alpha_0 \frac{P_\odot}{P_{\rm rot}} \quad \text{and} \quad f(\theta) = \cos\theta \sin^2\theta. \tag{8}$$

Note that the latitudinal emergence of the starspots is taken as a function of cos θ (to consider the effect of Coriolis force), and $\sin^2\theta$ is added to suppress the high-latitude emergence of the starspots.

In the second case, we have used the following dependence of rotation on the strength of the BL process, motivated by Kitchatinov & Olemskoy (2015):

Case II:

$$\alpha(\Omega) = \alpha_0 \frac{\sin\left(\alpha_\odot \frac{P_\odot}{P_{\rm rot}}\right)}{\sin\alpha_\odot} \quad \text{and} \quad f(\theta) = \cos\theta \sin^{2n}\theta, \tag{9}$$

where $\alpha_\odot$ is the average tilt angle observed for the Sun, and $n = P_{\rm rot}/P_\odot$. Here we have considered the rotational dependence on the emergence latitudes of starspots, which makes sure that if the star rotates faster, the starspots will have higher-latitude emergence. Note that if $P_{\rm rot}$ is equal to the solar rotation period, the α profile converges to the standard solar case. As we do not have an exact understanding of how latitudes of starspot emergence vary with the rotation, we just follow a simple profile to invoke the effect of rotation on the latitudinal emergence of starspots. The α profile for this case is shown in Figure 4 for a few stars.

3. Results

We run dynamo simulations for various stars with different rotation periods and mass of 1 $M_\odot$ and that have an outer CZ and a tachocline. Because the parameters, namely diffusivity and turbulent magnetic pumping, in the present dynamo model differ from the previous models available in the literature, we shall first present the results for the Sun.

3.1. The Sun

First, we make sure that with a chosen diffusivity, turbulent pumping, and BL α, a cyclic solar-type solution with 11 yr periodicity is reproduced. We find that, using the strength $\alpha_0 = 4.0$ m s^{-1} and pumping amplitude $\gamma_0 = 24$ m s^{-1}, a cyclic solution and all the basic properties of the solar magnetic field are well reproduced. In Figure 5, the basic features (e.g., equatorward migration, periodic cycle) of the solar magnetic fields are shown. The toroidal and radial fields are shown in the left and right panels of Figure 5, respectively. The equatorward migration and the correct phase relationship between the poloidal and toroidal fields are evident from the butterfly diagrams. A strong toroidal field appears at relatively higher latitudes than expected from the observations of sunspots. A high-latitude field is a consequence of the strong shear in the tachocline region at high latitudes. The high-latitude toroidal flux can partially be avoided by pushing the fields below the tachocline by the downward meridional flow (Nandy & Choudhuri 2002); however, our meridional flow does not penetrate below the tachocline. The five snapshots of toroidal and poloidal field lines are also shown in Figure 6 across an entire solar cycle. Filled contours show the toroidal fields, and the black solid and dashed contours show the poloidal fields at the same five instants of time.

A specific aspect of our solar dynamo solution is that the cycle period is about 13 yr. This time period is important not because this number is close to the solar cycle period, but rather that this was not expected given the value of the diffusivity (Equation (3)) used in our model. It is expected that the dynamo cycle period becomes shorter with increasing diffusivity (Dikpati & Charbonneau 1999; Hotta & Yokoyama 2010). In fact, the cycle period cannot be longer than the diffusion timescale of the magnetic field. That is why all previous flux transport dynamo models were built at much lower diffusivity to get the 11 yr period (Dikpati & Charbonneau 1999; Jouve et al. 2008). The exceptions were (1) the Surya model (Chatterjee et al. 2004; Jiang et al. 2007), in which the poloidal field diffusivity was reasonably high but the toroidal field diffusivity was much lower, and (2) the model of Kitchatinov & Olemskoy (2015), in which the diffusivity in the upper convection is high but much lower below 0.75 $R_\star$. In the present model, we get a longer period at relatively higher diffusivity because we use a downward magnetic pumping. As demonstrated in Cameron et al. (2012) and Karak & Cameron (2016), the pumping makes the magnetic field more radial near the surface and suppresses the diffusion of the flux across the surface. The weaker diffusion effectively increases the dynamo efficiency and allows dynamo action at a smaller value of α_0. This causes the cycle period to increase. Essentially what happens is that the poloidal field remains frozen in the CZ for a long time, and this allows the shear to produce a strong toroidal field that also does not diffuse across the surface and only diffuses across the equator (see Figure 6). This makes the cycle longer.

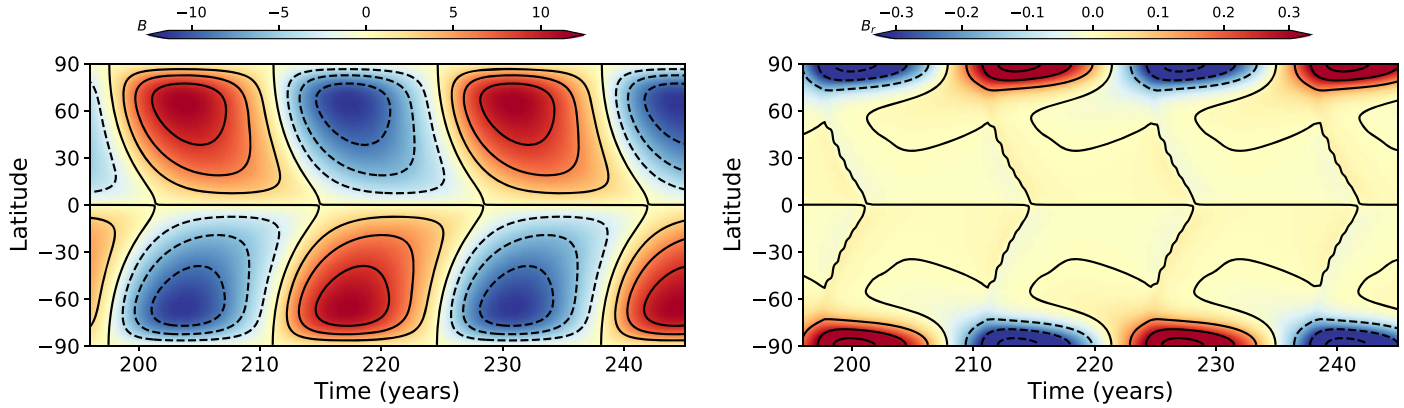

Figure 5. Time–latitude variation of the toroidal field at the bottom of the CZ ($r = 0.71R_\odot$; left panel) and the surface radial field (right panel). All magnetic fields are given in the unit of B_0.

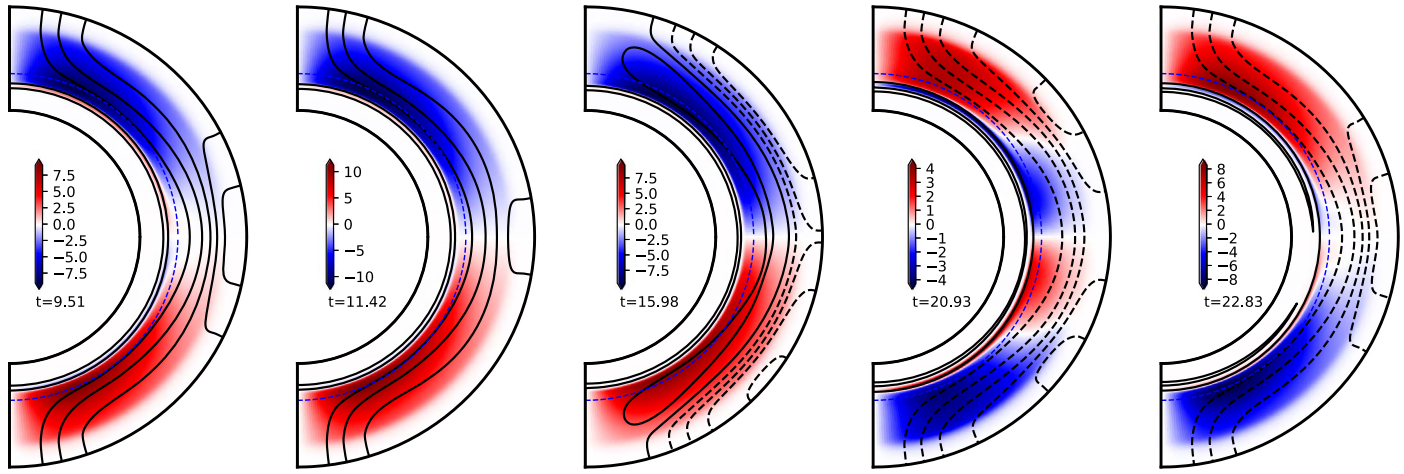

Figure 6. Dynamics of the field structure is shown for an entire solar cycle. Five snapshots are plotted at five different times in a solar cycle. The filled contours represent the toroidal field (in the unit of B_0), where blue and red colors show the negative and positive polarities, respectively. The black contours show the poloidal field lines (the solid line represents clockwise, and the dashed line shows the counterclockwise poloidal fields).

3.2. Stars with Different Rotation Periods

Now we present results of our simulations for different stars with different rotation periods. The mass of these stars is 1 $M_\odot$ and the rotation periods are 1, 2, 3, 5, 7, 10, 12, 15, 17, 20, 25.38 (the solar value), and 30 days. Since the rotation has a significant effect on the dynamics of the CZ, the mean flows and other turbulent transport coefficients are expected to be different for stars with different rotation periods. As discussed in the model section, the mean flows that we have used in our model are different for different stars (Kitchatinov & Olemskoy 2011a). But to avoid complexity, we consider the same turbulent diffusivity and pumping as that of the Sun (see Equations (4) and (5)) for all stars. Transport coefficients are also dependent on the magnetic field (Kitchatinov et al. 1994a; Karak et al. 2014c) and thus are expected to change with different stars. We, however, ignore these in our model. We now show the results of simulations with an α profile as given in Equation (8).

All of the stars in our sample show a systematic periodic variation in their activity cycle. Figure 7 shows the time–latitude diagrams of the toroidal magnetic field at $r = 0.71R_\star$ for six different stars. We believe that this toroidal field largely governs the dynamics of the starspots on the stellar surface. The slowly rotating stars with rotation period $\geqslant$17 days show some features that are in common with the Sun, particularly the equatorward migration of toroidal field and dipolar magnetic fields as shown in Figures 7(a) and (b). However, for the stars with a rotation period of 15 days and less, the equatorward migration turned into poleward migration and the parity changed to quadrupolar. The poleward migration is due to the dominant role of the dynamo wave over the meridional flow. As discussed in Section 2, with increasing rotation rate the meridional circulation becomes increasingly weaker and the transport of the toroidal field by the meridional flow becomes increasingly less effective (Figures 7(c)–(f)). When the rotation period decreased to 15 days, the toroidal band is completely dominated by poleward-propagating branches. These results are more or less insensitive to our chosen BL α profiles. Interestingly, for rapidly rotating stars, starspots are also observed in the higher latitudes. Therefore, the stronger toroidal fields (which are believed to produce the starspots) appearing at higher latitudes in our rapidly rotating stars are consistent with observations. However, a recent simulation by Işık et al. (2018) based on flux emergence and the surface flux transport (SFT) model shows the equatorward propagation of starspots even in the case of fast-rotating stars. This is presumably due to the solar-type time–latitude pattern of flux eruption that they have implemented at the base of the CZ in all solar-type stars, including the rapidly rotating stars. They have

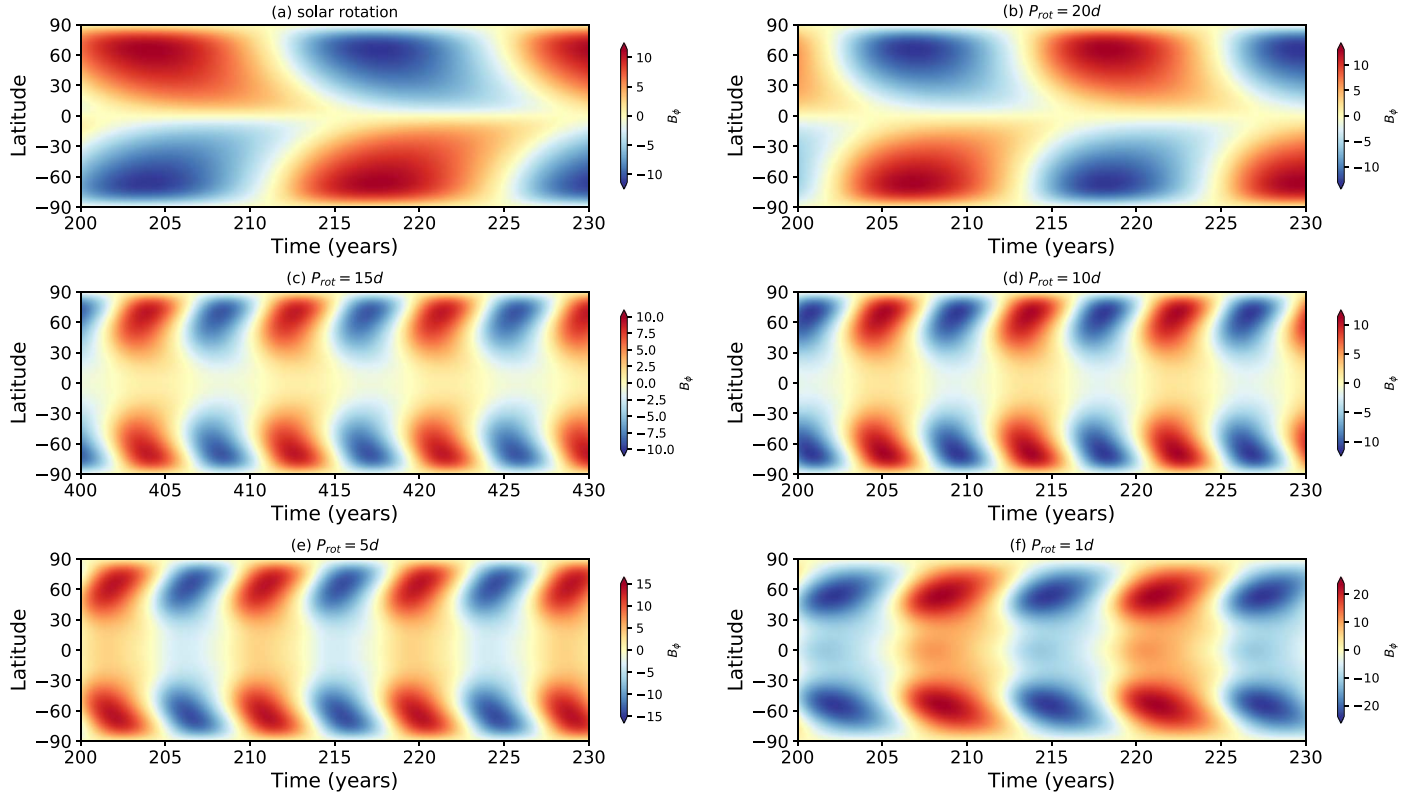

Figure 7. Time–latitude plots of toroidal field near the bottom of the CZ ($r = 0.71R_\star$) for different stars with rotation period of (a) the solar value, (b) 20 days, (c) 15 days, (d) 10 days, (e) 5 days, and (f) 1 day. All plots are for the α profile given in Equation (8).

also found that for fast-rotating stars, the activity the near-equatorial region is empty of activity because of flux-tube rise along the rotation axis. Our calculations find that for fast-rotating stars, the toroidal field near the equatorial region is less, due to cross-equatorial diffusion, but its effect is not negligible (see Figure 10).

3.3. Activity–Rotation Relation

Now we want to see whether our model can explain the observed variations of the Ca II H and K emission with rotation. The amount of Ca II H and K emission flux from the stellar chromosphere is a direct consequence of the magnetic heating in the stellar chromosphere, so it should be related to the total magnetic flux of the stars that is generated inside their CZs. We first measure the total amount of toroidal flux inside the stellar CZ as $fB_0R_\star^2$, where B_0 is the quenching field strength (same for all of our calculations), and then we consider the value f as a measure of total toroidal flux for all of the stars. As discussed in Karak et al. (2014b), the nonlinear quenching in α tries to limit the magnetic field in the model around B_0. Thus the stellar magnetic flux should be measured with respect to $B_0R_\star^2$. Obviously, if we plot f as a function of time, we find an oscillatory behavior, and its value during the cycle maxima would be maximum and we call it f_m. As the rotation of a star increases, we expect more field to be generated inside the stellar CZ, and that would lead to more Ca II H/K emission. Since the production of the emission generally involves magnetic reconnection of one flux system with another, we naively assume the emission goes as the square of the magnetic flux, that is, f_m^2, following Karak et al. (2014b). Vidotto et al. (2014) found the value of 1.8 ± 0.2 for the power index in the dependence of the X-ray luminosity on the large-scale (unsigned) magnetic flux (see the very short Section 3.1.4 and Figure 5 in their paper). As we have used two particular profiles of BL α depending on the rotational dependence as given in Case I (Equation (8)) and Case II (Equation (9)), we present results using both of them. The square of maximum toroidal flux amplitude (f_m^2) is plotted as a function of rotation period, which is shown in Figure 8(a) with α for Case I and α for Case II. In Figure 8(b), we plot the same square of maximum amplitude of the toroidal flux but with Rossby number instead of rotation period. Because our sample points spectrally belong to the G-type stars, both of the Figures 8(a) and (b) show a similar trend. As we see with both α profiles, the toroidal flux keeps on increasing with increasing rotation rate, but for the stars with rotation period less than 17 days (when parity flips from dipolar to quadrupolar), the total magnetic flux encounters diminution, and after that it again starts to rise. For the α profile chosen in Case II, we find a dip for the fast rotators with rotation period of 1 day, which is not found for the rotation profile of Case I.

The amplitude of the toroidal field, which determines the cycle strength, kept on increasing with increasing strength of the BL α. In both cases, the strength of α always increases with rotation, and the strength of the toroidal flux also kept on increasing. When parity changes from dipolar to quadrupolar for stars with rotation period less than 17 days, the cross-equatorial diffusion of toroidal flux across the hemispheres becomes more, and as a result we find a diminution in the toroidal field strength (see Figure 8). A slight dip, which is also found for the toroidal flux in fast-rotating stars for the α profile chosen in Case II, is due to the inclusion of tilt-angle saturation in the specified α profile. For Case I (Equation (8)), where

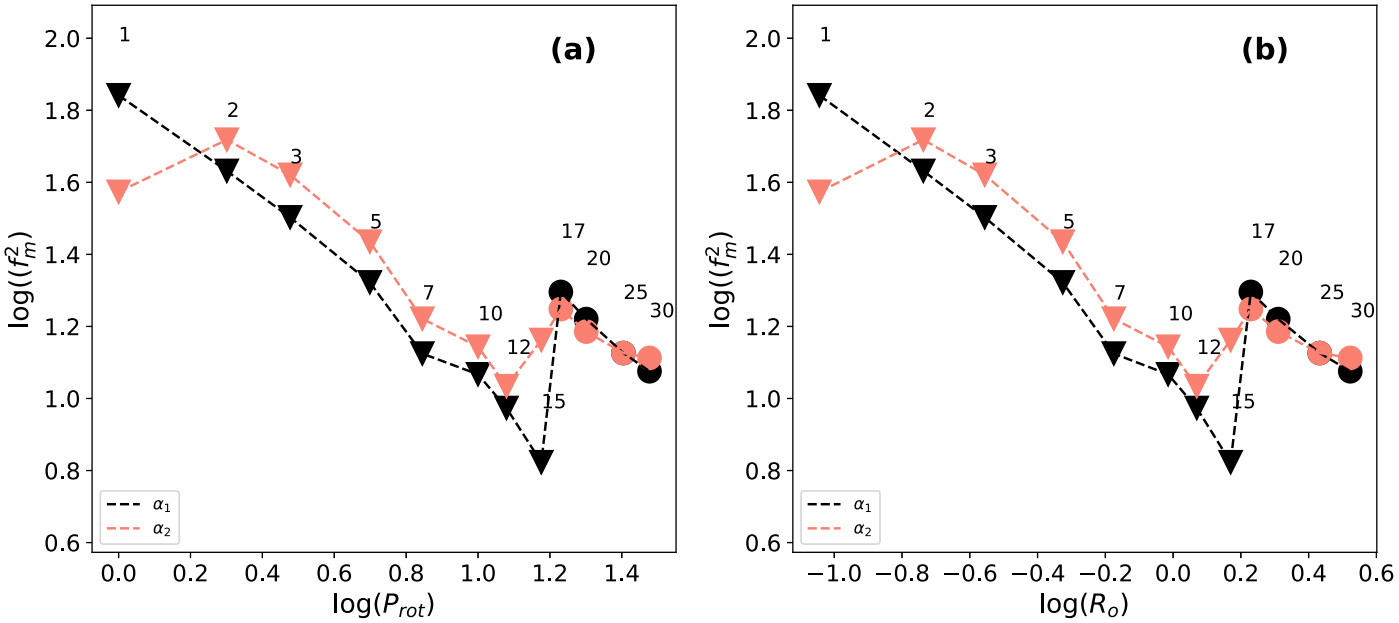

Figure 8. Peak amplitudes of the toroidal flux for different stars plotted as a function of (a) rotation period and (b) Rossby number. Two different curves in each plot are for two different α profiles (Equations (8) and (9)). Triangular and circular symbols show stars with quadrupolar and dipolar fields, respectively. Numbers on the plot represent the rotation period of each star.

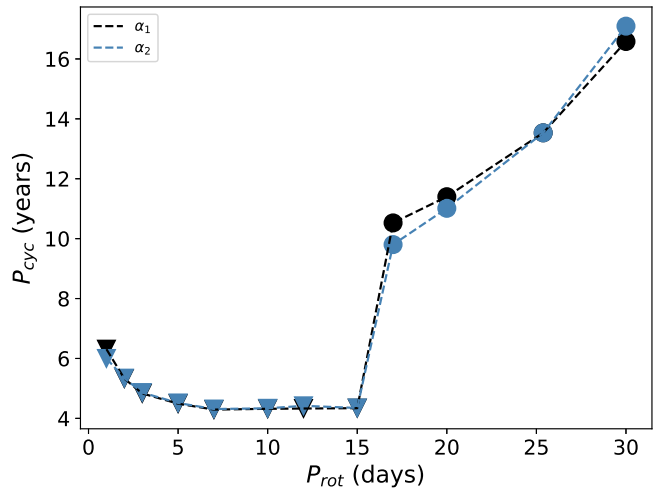

Figure 9. $P_{\rm rot}$ vs. $P_{\rm cyc}$ plot for two different α profiles used in our simulations. The black dashed line shows the case in which the α profile is chosen based on Equation (8). The blue dashed line shows the case in which the α profile is based on Equation (9). Triangular and circular symbols show stars with quadrupolar and dipolar parities, respectively.

rotational dependence on α is chosen as $\alpha(\Omega) = \alpha_0 \frac{P_\odot}{P_{\rm rot}}$, the strength of α always increases with rotation, and the strength of the toroidal flux also kept on increasing (black dashed line in Figures 8(a) and (b)). This is in accordance with the findings of Karak et al. (2014b) with the same rotational dependency on α. In Case II, we have chosen the saturation in the BL α profile (Equation (9)) motivated by observations. In principle, the tilt angle of the bipolar magnetic regions would increase with the rotation rate of a star. Also, we expect high-latitude emergence of the bipolar regions, that is, the radial rise of flux tubes for rapid rotation. All these properties of flux tube emergence are incorporated into the profile that we use for BL α as in Case II (Equation (9)). Incorporating tilt-angle saturation makes the poloidal fields be saturated for rapid rotators, and allowing the radial rise contributes less flux in the surface (Karak et al. 2014b), which gives rise to the dip in the highly rotating branch of the rotation–activity curve (Figure 8). As our model is presently kinematic, we have not considered the Lorentz force feedback on the mean flows of the stars (Hazra & Choudhuri 2017). The Lorentz force feedback for fast rotators most likely modulates the mean flows of those stars, which in turn modulate the total magnetic field of those stars.

3.4. P_{cyc}–P_{rot} Relation

We have also calculated the cycle periods based on the toroidal field reversals for different stars rotating with different rotation rates. The cycle period keeps on varying with increasing rotation rate or decreasing rotation period. In Figure 9, we have shown two cases with the two α profiles used in our model. For both of them, we find that the cycle period decreases with decreasing rotation period. For the stars with rotation periods less than 15 days, the cycle period increased very marginally, and for fast rotators (after rotation periods of 7 days), it started to increase considerably. The different symbols in the plot show the parity of the global magnetic field of the stars. Triangle symbols show the stars with quadrupolar parity, and filled circles show the stars with dipolar parity. Note that after the parity flips to quadrupolar for stars with rotation periods less than or equal to 15 days, the cycle periods started to increase. Overall, our results are consistent with the observed $P_{\rm cyc}$–$P_{\rm rot}$ relation. We find a decreasing trend of cycle periods with increasing rotation rate for slowly rotating stars, as found by Boro Saikia et al. (2018; see Figure 9 of their paper). For the fast-rotating stars, there is no clear observed trend of how cycle period behaves with the rotation rate of the stars, and our results provide some crucial evidence. As mentioned earlier, in all of our simulations, we have not changed the transport coefficients (turbulent diffusivity and turbulent pumping), which may make a significant contribution to setting up the cycle period. So far, we do not have a clear indication of how these transport coefficients

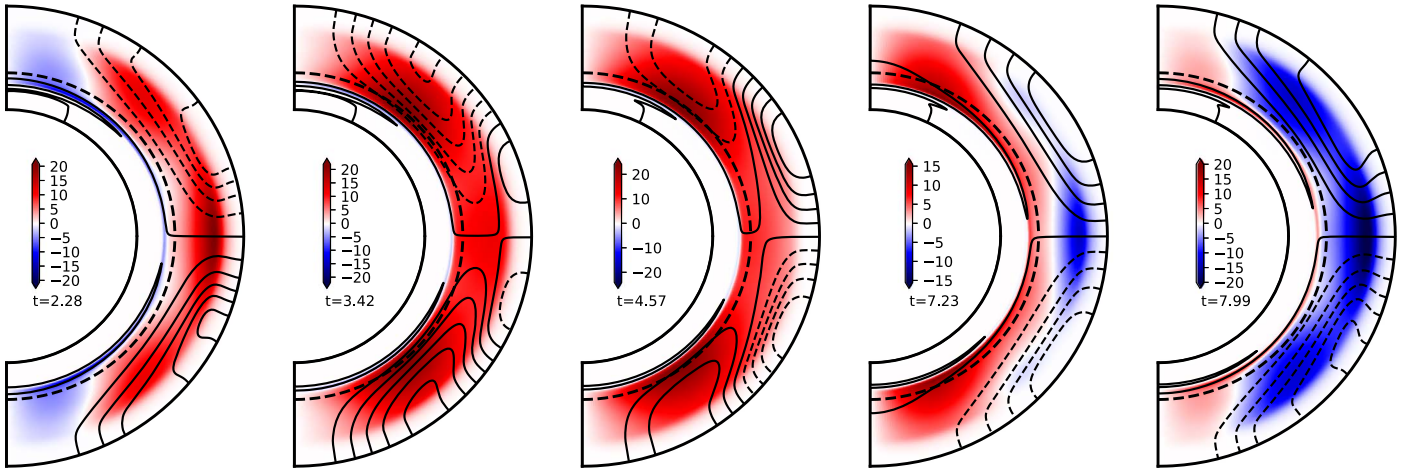

Figure 10. Same as Figure 6 but for the star with rotation period of 1 day.

will vary with the rotation, and we just keep everything constant with rotation. The blue dashed line in Figure 9 shows the cycle period as a function of rotation period for the α in Case II (Equation (9)). It shows a behavior similar to the black dashed line that has the same pumping amplitude but different α (Case I, Equation (8)). Hence, the $P_{\rm cyc}$–$P_{\rm rot}$ relation is robust under the variation in the chosen profiles of α.

Previous efforts (Jouve et al. 2010; Dubé & Charbonneau 2013; Karak et al. 2014b) to model magnetic activity for solar-type stars were not able to get the correct trend of cycle period with rotation. However, Do Cao & Brun (2011) found the decreasing trend of cycle period with increasing rotation rate by incorporating rotation-dependent radial and equatorward turbulent pumping inside the whole CZ. Unlike Do Cao & Brun (2011), we have incorporated only radial pumping near the surface and have chosen a high magnetic diffusivity inside the stellar CZ. In our model, the cycle period is dominated by radial turbulent pumping and turbulent diffusion. For the sample of stars that we have selected, apart from the varying rotation rate, the main parameters that change to affect the cycle period are the meridional flow and the strength of BL α. But in the presence of turbulent radial pumping and high turbulent diffusivity, the cycle period becomes less dependent on the meridional flow. When the rotation rate increases, the differential rotation or the shear becomes very strong, allowing generation of more toroidal fields, which in turn helps more poloidal fields to be produced. Since the strength of the α parameter also increases with increasing rotation rate, the fast-rotating stars have more poloidal field to reverse the existing toroidal field, which makes the cycle shorter (Karak & Cameron 2016). This trend is clear from our simulations. As the rotation rate of a star increases, the period of the cycle tends to be shorter, and the amplitude becomes stronger. For stars with rotation periods less than 15 days, there is a trend of a slight increase in cycle period with decreasing rotation period. The radial shear becomes weak for those stars, and it takes more time to generate the opposite-polarity toroidal fields by twisting the poloidal fields, which affects the timescale of polarity reversal and hence the cycle periods.

3.5. Parity

Another intriguing result obtained from our simulations is the change in stellar magnetic field parity with rotation. The parity becomes quadrupolar for the stars with rotation period less than 17 days. We have not run our simulations for many rotation periods to determine the exact rotation period after which the magnetic fields flip to quadrupolar, but qualitatively we find that if the rotation periods are less than 17 days, the stellar magnetic field becomes quadrupolar. The parity of the global magnetic field of stars is determined by various turbulent transport coefficients inside the stellar CZ. Whether the parity of the stellar magnetic field is dipolar or quadrupolar is mainly decided by two factors: first, how the toroidal field inside the CZ couples with the opposite hemisphere, and second, how efficient is the equatorward mixing of the poloidal field near the surface. To keep the magnetic field antisymmetric across the equator, that is, to keep dipolar parity, the hemisphere coupling of the toroidal fields should be much less. Usually, the amount of turbulent diffusivity used in the solar CZ is two orders of magnitude less than its value near the surface, and the cross-equatorial diffusion of toroidal fluxes is much less, which makes sure that the polarities of the toroidal fields in the two hemispheres remain opposite to each other. Also, as the BL mechanism is confined near the surface, good hemisphere mixing is necessary near the equator to lead polarity starspots to cancel each other out. That requires a high value of turbulent diffusion near the surface to maintain the dipolar parity.

In our present model, we have used a high diffusivity value inside the CZ and a turbulent radial pumping near the surface. Turbulent radial pumping near the surface and a radial boundary condition in our model make the field lines radial near the surface and do not allow diffusive decay of fields through the surface. So in this situation fields can only diffuse through the equator. But for fast-rotating stars, the poloidal field does not get enough time to diffuse across the equator because the cycle period becomes shorter as a star rotates faster. Also, for fast-rotating stars, the strong poloidal field is generated at very high latitude, which does not give enough time for the diffusive mixing across the equator. As a result, the fast-rotating stars turn out to have a quadrupolar polarity. The lower diffusion of the poloidal field near the equator makes the new toroidal field symmetric across the equator. Therefore, for rapidly rotating stars (e.g., $P_{\rm rot} = 1$ day), the equatorward cancellation of the poloidal field is not that efficient (see poloidal field lines of Figure 10), which in turn favors the quadrupolar mode. Observationally, it is very difficult to

quantify the correct parity of the stellar magnetic fields, due to instrument limitations, and there were no direct observed results until now about the correct parity of the stars. Our simulations provide very important information in this area about the correct parity of the stars.

In summary, the most important results that we have obtained from our simulations are as follows. (1) The global magnetic fields of the stars tend to be quadrupolar for rapidly rotating stars; more precisely, in all of our simulations, we get quadrupolar parity in stars whose rotation periods are less than or equal to 15 days. (2) The cycle period decreases as the rotation rate of the star increases, and after a rotation period of 15 days, there is an increasing trend in cycle period as the rotation rate of the star increases. (3) The magnetic activity increases as the rotation rate of the star starts to increase. The first two results are new results and new achievements from our model. Previously, Do Cao & Brun (2011) were able to reproduce the decreasing trend of cycle period with increasing rotation rate, but they had to assume a rotation-dependent turbulent pumping throughout the CZ that scales as Ω^2, and their equatorial pumping was strong compared to the radial pumping. In contrast, we have assumed only a constant radial pumping near the surface layers of the stars, which is more physical and consistent with previous studies (Miesch & Hindman 2011; Cameron et al. 2012; Jiang et al. 2013).

Both of these results (quadrupolar fields and $P_{\rm cyc}$–$P_{\rm rot}$ relation) are robust under reasonable changes in the parameters adopted in our models. The overall behavior of the results remains the same if we vary the amplitude of the turbulent pumping. We run a few cases for all stars considering a range of turbulent pumping amplitudes from 16 to 36 m s^{-1} and find that each case gives a similar trend in the results. However, if the pumping amplitude is reduced below 16 m s^{-1}, then the decrease in cycle period with the increase in rotation rate disappears. We have also performed some of the simulations by changing the pumping amplitude with rotation. Notably, the set of simulations in which the turbulent pumping is quenched linearly with the rotation period also produce similar behaviors. The dynamo saturation for the rapidly rotating stars was explained earlier (Jouve et al. 2010; Karak et al. 2014b; Kitchatinov & Olemskoy 2015), but we present it here to support the idea that dynamo saturation might be a result of saturation in the BL mechanism, and we find an indication of the dynamo saturation using our α profiles given in Case II. For Case II, we have used the similar profile motivated by Kitchatinov & Olemskoy (2015, see Equation (9)), and we find quite similar results. One of the other possibilities of the dynamo saturation might be the Lorentz force feedback on the mean flows, which we could not explore in our model because of its kinematic nature.

4. Conclusions

In this paper, we have utilized a kinematic flux transport dynamo model with BL α as the poloidal source to explain the features of the magnetic fields and cycles of solar-type stars with mass 1 $M_\odot$. Our dynamo model is different than the traditional flux transport dynamo models in the sense that our model includes a significant downward magnetic pumping that mimics strong asymmetric surface convection (Miesch & Hindman 2011). This magnetic pumping suppresses the diffusion of the horizontal magnetic field through the surface and thus makes the behavior of the dynamo different from traditional flux transport dynamos (Cameron et al. 2012; Jiang et al. 2013; Karak & Cameron 2016; Karak & Miesch 2017, 2018). In our dynamo model, large-scale flows such as differential rotation and meridional circulation are taken from the hydrodynamic mean-field models (Kitchatinov & Olemskoy 2011a) of the corresponding stars. The back reaction of the magnetic field on the flow has been ignored in this model. In all our simulations, we have used a higher diffusivity in the CZ ($\eta_{\rm CZ} = 7.5 \times 10^{11}$ cm^2 s^{-1}) than the traditional flux transport dynamo model, where they use 5×10^{10} cm^2 s^{-1} (Dikpati & Charbonneau 1999; Miesch & Dikpati 2014). Some exceptions are Chatterjee et al. (2004) and Hazra et al. (2014), who use different diffusivities corresponding to poloidal and toroidal fields.

The α profile is changed in two different ways. In one case, only the amplitude of the α profile is scaled up with the rotation rate (Case I; Equation (8)), while in the other case, the mean sunspot tilt is scaled up with the rotation rate, and the latitudinal profile of the α is increased with the rotation rate such that with the increase in the rotation rate, the region of generation of the poloidal field is progressively moved to higher latitudes (Case II; Equation (9)). The latter case is more physical because we know that in the BL process, the average tilt (λ) of bipolar magnetic regions (BMRs) largely determines the poloidal field. Thus, BL α should be proportional to $\sin(\lambda)$. The BMR tilt is expected to increase with the rotation rate (due to the increase in Coriolis force as suggested in thin flux tube simulations; D'Silva & Choudhuri 1993; Fan et al. 1993). Observations also suggest that the starspots appear in higher latitudes (Jeffers et al. 2002; Marsden et al. 2006; Waite et al. 2015), and thus we expect that the region of the poloidal field generation would be more concentrated toward high latitudes for rapidly rotating stars.

An interesting result of our study is that the cycle period decreases with the increase in the rotation rate of a star for slowly rotating stars, and the cycle period starts to increase for a star whose rotation period is shorter than 15 days. This result is in agreement to a greater extent with the available observed magnetic activity of solar-type stars (Noyes et al. 1984b; Suárez Mascareño et al. 2016; Boro Saikia et al. 2018). This result also is in striking contrast to the previous studies based on the traditional flux transport dynamo models (Jouve et al. 2010; Karak et al. 2014b). As the meridional circulation becomes weaker in the rapidly rotating stars, we expect the cycle period to be longer. However, in our model, the downward magnetic pumping does not allow the field to diffuse across the surface, and thus the field can only diffuse across the equator. And as the rotation of the stars starts to increase, the poloidal field becomes stronger, which takes less time to reverse the toroidal field faster, reducing the cycle period.

The most appealing result of our study is that the magnetic field changes its parity from dipolar to quadrupolar in rapidly rotating stars of rotation period less than 17 days. In the rapidly rotating stars, a shorter cycle period (as discussed above) gives less time to diffuse the field. The lower diffusion of the poloidal field across the equator keeps the poloidal field from connecting, which is essential to keeping the field dipolar. This inefficient mixing of the poloidal field across the equator near the surface makes the magnetic field quadrupolar in rapidly rotating stars of periods less than about 17 days. Thus, our simulations predict a quadrupolar field in rapidly rotating stars.

Another important result of our study is that the magnetic activity increases with the increase in rotation rate associated with a small dip at the rotation period of 15 days. In Case II of the α profile, we find a slight indication of saturation of magnetic field, in agreement with Kitchatinov & Olemskoy (2015). The increase in magnetic activity in our model is in broad agreement with observations (Noyes et al. 1984a; Wright et al. 2011; Vidotto et al. 2014; Suárez Mascareño et al. 2016).

Although our results are robust under some variations in the parameters (e.g., BL α and turbulent pumping), we have some limitations in our study. We have not explored a wide range of the diffusivity profile. The turbulent diffusivity even for the Sun is not well constrained. Theoretical and observational arguments (Chae et al. 2008; Muñoz-Jaramillo et al. 2011; Cameron & Schüssler 2016; Hazra & Miesch 2018) suggest that in the surface layer it is at least 10^{12} cm^2 s^{-1} and in the deeper CZ it is probably less. However, we have limited knowledge of how it varies with the rotation rate and the magnetic field strength in other stars (e.g., Kitchatinov et al. 1994b; Karak et al. 2014c). Therefore, a drastic change in the turbulent diffusivity (and also in the magnetic pumping) may alter our conclusions reported in this study. Our model is kinematic, meaning we have ignored the feedback of the magnetic field on the large-scale flows. But for the Sun this is probably not a bad approximation because the variation in the differential rotation with the magnetic cycle is very tiny. However, this may not be a good assumption in rapidly rotating stars in which the magnetic field is much stronger. Similarly, we have neglected the turbulent α effect, which (in comparison to the BL α) is probably insignificant in the Sun but may be important in rapidly rotating stars (Karak & Tomar 2019). Furthermore, we have not considered the small-scale magnetic field that could be generated through the small-scale dynamo, which may become important in giving some nonthermal emission in the chromospheres of rapidly rotating stars. Finally, we have not considered any possible sources of the variations in the magnetic field (e.g., fluctuations in the BL process due to variations in the tilt angle and the variation in the meridional circulations). Observations show that many stars show irregular cycles and possibly extended grand minima (Saar & Testa 2012). Thus, the irregular aspects should be carefully studied and checked whether the solar dynamo models (Karak & Choudhuri 2011; Hazra et al. 2015; Kitchatinov et al. 2018), which are successful in explaining many irregular aspects of the solar cycle, are capable of explaining the irregular features of other stars. However, seeing the success in reproducing many observational features of stellar cycles in our model, we can have some confidence in the basic assumptions made in our model, and we expect that the prediction made for the quadrupolar field in rapidly rotating stars is true. We hope that future stellar observations will validate our prediction.

We thank an anonymous referee for constructive comments that helped to improve the manuscript. It is our pleasure to thank Prof. Arnab Rai Choudhuri for various discussions that helped us a lot to work on this project. G.H. thanks Prof. Aline Vidotto for several discussions related to this work. G.H. and J.J. acknowledge the support by the National Science Foundation of China (grant Nos. 11873023 and 11522325) and by the Fundamental Research Funds for the Central Universities of China. B.B.K. sincerely thanks SERB/DST, India, for providing a research grant through the Ramanujan Fellowship (project No. SB/S2/RJN-017/2018). B.B.K. further thanks Janardhan Padmanabhan and Aveek Sarkar for providing the warm hospitality in the Physical Research Laboratory, Ahmedabad, where he did some revision of this paper. L.K. acknowledges the support by the Russian Foundation for Basic Research (project 17-52-80064) and by budgetary funding of Basic Research program II.16.

ORCID iDs

Gopal Hazra https://orcid.org/0000-0001-5388-1233
Jie Jiang https://orcid.org/0000-0001-5002-0577
Bidya Binay Karak https://orcid.org/0000-0002-8883-3562

References

Babcock, H. W. 1961, ApJ, 133, 572
Barnes, J. R., Collier Cameron, A., Donati, J.-F., et al. 2005, MNRAS, 357, L1
Berdyugina, S. V. 2005, LRSP, 2, 8
Böhm-Vitense, E. 2007, ApJ, 657, 486
Boro-Saikia, S., Marvin, C. J., Jeffers, S. V., et al. 2018, A&A, 616, A108
Brown, B. P., Browning, M. K., Brun, A. S., Miesch, M. S., & Toomre, J. 2008, ApJ, 689, 1354
Brun, A. S. 2014, in IAU Symp. 302, Magnetic Fields throughout Stellar Evolution, ed. P. Petit, M. Jardine, & H. C. Spruit (Cambridge: Cambridge Univ. Press), 114
Cameron, R., & Schüssler, M. 2015, Sci, 347, 1333
Cameron, R. H., Schmitt, D., Jiang, J., & Işık, E. 2012, A&A, 542, A127
Cameron, R. H., & Schüssler, M. 2016, A&A, 591, A46
Chae, J., Litvinenko, Y. E., & Sakurai, T. 2008, ApJ, 683, 1153
Charbonneau, P. 2010, LRSP, 7, 3
Chatterjee, P., Nandy, D., & Choudhuri, A. R. 2004, A&A, 427, 1019
Choudhuri, A. R. 2011, Prama, 77, 77
Choudhuri, A. R. 2017, SCPMA, 60, 19601
Choudhuri, A. R., Schüssler, M., & Dikpati, M. 1995, A&A, 303, L29
Dasi-Espuig, M., Solanki, S. K., Krivova, N. A., Cameron, R., & Peñuela, T. 2010, A&A, 518, A7
DeRosa, M. L., Brun, A. S., & Hoeksema, J. T. 2012, ApJ, 757, 96
Dikpati, M., & Charbonneau, P. 1999, ApJ, 518, 508
Do Cao, O., & Brun, A. S. 2011, AN, 332, 907
D'Silva, S., & Choudhuri, A. R. 1993, A&A, 272, 621
Dubé, C., & Charbonneau, P. 2013, ApJ, 775, 69
Durney, B. R. 1995, SoPh, 160, 213
Durney, B. R., & Robinson, R. D. 1982, ApJ, 253, 290
Fan, Y., Fisher, G. H., & Deluca, E. E. 1993, ApJ, 405, 390
Guerrero, G., & de Gouveia Dal Pino, E. M. 2008, A&A, 485, 267
Guerrero, G., Smolarkiewicz, P. K., Kosovichev, A. G., & Mansour, N. N. 2013, ApJ, 779, 176
Hale, G. E., Ellerman, F., Nicholson, S. B., & Joy, A. H. 1919, ApJ, 49, 153
Hazra, G., & Choudhuri, A. R. 2017, MNRAS, 472, 2728
Hazra, G., Karak, B. B., Banerjee, D., & Choudhuri, A. R. 2015, SoPh, 290, 1851
Hazra, G., Karak, B. B., & Choudhuri, A. R. 2014, ApJ, 782, 93
Hazra, G., & Miesch, M. S. 2018, ApJ, 864, 110
Hotta, H., & Yokoyama, T. 2010, ApJL, 714, L308
Hotta, H., & Yokoyama, T. 2011, ApJ, 740, 12
Işık, E., Solanki, S. K., Krivova, N. A., & Shapiro, A. I. 2018, A&A, 620, A177
Jeffers, S. V., Barnes, J. R., & Collier Cameron, A. 2002, MNRAS, 331, 666
Jiang, J., Cameron, R. H., Schmitt, D., & Işık, E. 2013, A&A, 553, A128
Jiang, J., Cameron, R. H., & Schüssler, M. 2014, ApJ, 791, 5
Jiang, J., Cameron, R. H., & Schüssler, M. 2015, ApJL, 808, L28
Jiang, J., Chatterjee, P., & Choudhuri, A. R. 2007, MNRAS, 381, 1527
Jouve, L., Brown, B. P., & Brun, A. S. 2010, A&A, 509, A32
Jouve, L., Brun, A. S., Arlt, R., et al. 2008, A&A, 483, 949
Käpylä, M. J., Käpylä, P. J., Olspert, N., et al. 2016, A&A, 589, A56
Käpylä, P. J., Korpi, M. J., Ossendrijver, M., & Stix, M. 2006, A&A, 455, 401
Karak, B. B. 2010, ApJ, 724, 1021
Karak, B. B., & Cameron, R. 2016, ApJ, 832, 94
Karak, B. B., & Choudhuri, A. R. 2011, MNRAS, 410, 1503
Karak, B. B., Jiang, J., Miesch, M. S., Charbonneau, P., & Choudhuri, A. R. 2014a, SSRv, 186, 561
Karak, B. B., Käpylä, P. J., Käpylä, M. J., et al. 2015, A&A, 576, A26
Karak, B. B., Kitchatinov, L. L., & Choudhuri, A. R. 2014b, ApJ, 791, 59
Karak, B. B., & Miesch, M. 2017, ApJ, 847, 69

Karak, B. B., & Miesch, M. 2018, ApJL, 860, L26
Karak, B. B., Miesch, M., & Bekki, Y. 2018, PhFl, 30, 046602
Karak, B. B., & Nandy, D. 2012, ApJL, 761, L13
Karak, B. B., Rheinhardt, M., Brandenburg, A., Käpylä, P. J., & Käpylä, M. J. 2014c, ApJ, 795, 16
Karak, B. B., & Tomar, A. 2019, MNRAS, submitted
Kitchatinov, L. L., Mordvinov, A. V., & Nepomnyashchikh, A. A. 2018, A&A, 615, A38
Kitchatinov, L. L., & Olemskoy, S. V. 2011a, MNRAS, 411, 1059
Kitchatinov, L. L., & Olemskoy, S. V. 2011b, AstL, 37, 656
Kitchatinov, L. L., & Olemskoy, S. V. 2012, SoPh, 276, 3
Kitchatinov, L. L., & Olemskoy, S. V. 2015, RAA, 15, 1801
Kitchatinov, L. L., Pipin, V. V., & Ruediger, G. 1994a, AN, 315, 157
Kitchatinov, L. L., Rüdiger, G., & Küker, M. 1994b, A&A, 292, 125
Kitchatinov, L. L., & Ruediger, G. 1995, A&A, 299, 446
Küker, M., & Stix, M. 2001, A&A, 366, 668
Leighton, R. B. 1969, ApJ, 156, 1
Marsden, S. C., Donati, J.-F., Semel, M., Petit, P., & Carter, B. D. 2006, MNRAS, 370, 468
Miesch, M. S. 2005, LRSP, 2, 1
Miesch, M. S., & Dikpati, M. 2014, ApJL, 785, L8
Miesch, M. S., & Hindman, B. W. 2011, ApJ, 743, 79
Muñoz-Jaramillo, A., Dasi-Espuig, M., Balmaceda, L. A., & DeLuca, E. E. 2013, ApJL, 767, L25
Muñoz-Jaramillo, A., Nandy, D., & Martens, P. C. H. 2011, ApJL, 727, L23
Nandy, D., & Choudhuri, A. R. 2002, Sci, 296, 1671
Noyes, R. W., Hartmann, L. W., Baliunas, S. L., Duncan, D. K., & Vaughan, A. H. 1984a, ApJ, 279, 763
Noyes, R. W., Weiss, N. O., & Vaughan, A. H. 1984b, ApJ, 287, 769
Olspert, N., Lehtinen, J. J., Käpylä, M. J., Pelt, J., & Grigorievskiy, A. 2018, A&A, 619, A6
Priyal, M., Banerjee, D., Karak, B. B., et al. 2014, ApJL, 793, L4
Racine, É., Charbonneau, P., Ghizaru, M., Bouchat, A., & Smolarkiewicz, P. K. 2011, ApJ, 735, 46
Rempel, M. 2005, ApJ, 622, 1320
Réville, V., Brun, A. S., Matt, S. P., Strugarek, A., & Pinto, R. F. 2015, ApJ, 798, 116
Robinson, R. D., & Durney, B. R. 1982, A&A, 108, 322
Saar, S. 2002, in ASP Conf. Ser. 277, Stellar Coronae in the Chandra and XMM-NEWTON Era, ed. F. Favata & J. J. Drake (San Francisco, CA: ASP), 311
Saar, S. H., & Brandenburg, A. 1999, ApJ, 524, 295
Saar, S. H., & Testa, P. 2012, in IAU Symp. 286, Comparative Magnetic Minima: Characterizing Quiet Times in the Sun and Stars, ed. C. H. Mandrini & D. F. Webb (Cambridge: Cambridge Univ. Press), 335
Schrijver, C. J., Dobson, A. K., & Radick, R. R. 1992, A&A, 258, 432
Schuessler, M., & Solanki, S. K. 1992, A&A, 264, L13
Skumanich, A., Smythe, C., & Frazier, E. N. 1975, ApJ, 200, 747
Stenflo, J. O. 1988, Ap&SS, 144, 321
Strassmeier, K. G. 2009, A&ARv, 17, 251
Strugarek, A., Beaudoin, P., Charbonneau, P., Brun, A. S., & do Nascimento, J. D. 2017, Sci, 357, 185
Suárez Mascareño, A., Rebolo, R., & González Hernández, J. I. 2016, A&A, 595, A12
Tobias, S. M., Brummell, N. H., Clune, T. L., & Toomre, J. 2001, ApJ, 549, 1183
Vidotto, A. A., Gregory, S. G., Jardine, M., et al. 2014, MNRAS, 441, 2361
Waite, I. A., Marsden, S. C., Carter, B. D., et al. 2015, MNRAS, 449, 8
Warnecke, J. 2018, A&A, 616, A72
Wright, N. J., & Drake, J. J. 2016, Natur, 535, 526
Wright, N. J., Drake, J. J., Mamajek, E. E., & Henry, G. W. 2011, ApJ, 743, 48